

## DIRECT DETECTION AND ORBIT ANALYSIS OF THE EXOPLANETS HR 8799 bcd FROM ARCHIVAL 2005 KECK/NIRC2 DATA

THAYNE CURRIE<sup>1</sup>, MISATO FUKAGAWA<sup>2</sup>, CHRISTIAN THALMANN<sup>3</sup>, SOKO MATSUMURA<sup>4</sup>, PETER PLAVCHAN<sup>5</sup>

*Draft version May 25, 2018*

### ABSTRACT

We present previously unpublished July 2005 *H*-band coronagraphic data of the young, planet-hosting star HR 8799 from the newly-released Keck/NIRC2 archive. Despite poor observing conditions, we detect three of the planets (HR 8799 bcd), two of them (HR 8799 bc) without advanced image processing. Comparing these data with previously published 1998-2011 astrometry and that from re-reduced October 2010 Keck data constrains the orbits of the planets. Analyzing the planets' astrometry separately, HR 8799 d's orbit is likely inclined at least 25° from face-on and the others may be on in inclined orbits. For semimajor axis ratios consistent with a 4:2:1 mean-motion resonance, our analysis yields precise values for HR 8799 bcd's orbital parameters and strictly constrains the planets' eccentricities to be less than 0.18–0.3. However, we find no acceptable orbital solutions with this resonance that place the planets in face-on orbits; HR 8799 d shows the largest deviation from such orbits. Moreover, few orbits make HR 8799 d coplanar with b and c, whereas dynamical stability analyses used to constrain the planets' masses typically assume coplanar and/or face-on orbits. This paper illustrates the significant science gain enabled with the release of the NIRC2 archive.

*Subject headings:* planetary systems, stars: early-type, stars: individual: HR 8799

### 1. INTRODUCTION

The nearby, young A-type star HR 8799 ( $d = 39.4$  pc,  $\approx 30$  Myr; Zuckerman et al. 2011) harbors the first independently confirmed, directly imaged exoplanetary system and the only imaged multi-planet system (Marois et al. 2008). After the discovery of HR 8799 bcd ( $r_{\text{proj}} \approx 24, 38,$  and  $68$  AU) reported in November 2008 (Marois et al. 2008), other studies identified at least one of these planets in archival data taken prior to 2008 (Lafrenière et al. 2009; Fukagawa et al. 2009; Metchev et al. 2009; Soummer et al. 2011).

HR 8799 planet astrometry derived from both pre and post-discovery images can help constrain the system's dynamical stability and, in turn, the planets' physical properties. At least two of the HR 8799 planets are likely locked in a mean motion resonance, otherwise the system would quickly become dynamically unstable (Fabrycky and Murray-Clay 2010). The recently discovered fourth companion at  $\sim 15$  AU, HR 8799 e, generally makes dynamical stability less likely (Marois et al. 2010a; Currie et al. 2011a), favoring lower masses of  $M_{\text{b,c,d,e}} < 7, 10 M_{\text{J}}$ , an important constraint given the uncertainties in deriving masses from planet cooling and atmosphere models (Spiegel and Burrows 2012; Madhusudhan et al. 2011).

Studies focused on fitting the planets' orbits and/or testing dynamical stability typically assume that the planets are a) in resonance (4:2:1 for HR 8799 bcd or 2:1 for HR 8799 cd), b) in circular, face-on orbits, c) and/or in coplanar orbits (e.g. Marois et al. 2010a;

Currie et al. 2011a, see also Fabrycky and Murray-Clay 2010). However, Soummer et al. (2011) show that circular, face-on, and coplanar orbits are inconsistent with 1998 HST astrometry, identifying a best-fit orbit for HR 8799 d of  $i = 28^\circ$  and  $e = 0.115$ . Generally, more eccentric orbits destabilize the system. The system stability depends on the (mutual) inclinations of the planets (Fabrycky and Murray-Clay 2010; Sudol and Haghighipour 2012). Thus, the HR 8799 planets' true mass limits derived from dynamical stability arguments may slightly differ from those previously reported.

Well-sampled HR 8799 d astrometry could help clarify whether HR 8799 d's orbit must be inclined, eccentric, and/or coplanar with the other planets. However, until now there is a  $\sim 9$ -year gap between the 1998 HST detection and the next one (2007; Metchev et al. 2009). New astrometry for HR 8799 bce in between 1998 and 2007 could also help constrain those planets' orbits. By better determining the HR 8799 planets' orbital properties, we can more conclusively investigate system dynamical stability and thus better clarify the range of allowable planet masses.

In this Letter, we report the detection of HR 8799 bcd from unpublished, now-public Keck/NIRC2 data taken in 2005 supplemented with a re-reduction of published October 2010 data from Marois et al. (2010a). We use these data to better constrain the orbital properties of HR 8799 bcd.

### 2. OBSERVATIONS AND DATA REDUCTION

#### 2.1. July 2005 Data

We downloaded HR 8799 data taken on July 15, 2005 from the newly-available Keck/NIRC2 data archive (Program ID H53BN2, P.I. Michael Liu). The data were taken in *H* band with the narrow camera (9.952 mas/pixel; Yelda et al. 2010) with the 0.6 diameter coro-

<sup>1</sup> NASA-Goddard Space Flight Center

<sup>2</sup> Osaka University

<sup>3</sup> Astronomical Institute Anton Pannekoek, University of Amsterdam

<sup>4</sup> Department of Astronomy, University of Maryland-College Park

<sup>5</sup> NExScI, California Institute of Technology

nagraphic spot and the “incircle” pupil plane mask. HR 8799 was observed in 10s exposures in “vertical angle” or *angular differential imaging* mode (Marois et al. 2006) through transit (Hour Angle =  $[-0.20, 0.55]$ ) with a total field rotation of  $147.1^\circ$ . During these observations, the seeing conditions fluctuated and the observers periodically recentered the star behind the mask, changing the intensity profile of the stellar halo (and thus the quasi-static speckle pattern). During a few frames near transit the star did not properly center at all behind the coronagraph. We identify  $\sim 11$  minutes of science-grade data. Basic image processing followed standard steps previously used to process NIRC2 data (Currie et al. 2012).

For a first-order reduction, we perform a simple “classical” ADI-based PSF subtraction (e.g. Marois et al. 2006). Figure 1 shows this reduction, clearly revealing HR 8799 b (SNR  $\sim 12$ ) and identifying HR 8799 c, albeit at low SNR ( $\sim 4$ ). With the LOCI approach (Lafrenière et al. 2007) as implemented and modified in previous work (Currie et al. 2010, 2011a,b), we easily detect HR 8799 b and c and obtain a marginal detection of HR 8799 d at  $r \sim 0''.6$  several degrees away (clockwise) from the July 2007 position reported by Metchev et al. (2009) (not shown).

To improve the signal-to-noise of our HR 8799 d detection, we incorporated several upgrades to enhance contrast which are being implemented in a new “adaptive” LOCI (A-LOCI) pipeline (T. Currie, 2012 in prep.; see also similar steps in Marois et al. 2010b). We subtract off the seeing halo in each image to measure the static/quasi-static speckle pattern, determining the cross-correlation function for the speckle patterns in annular sections for all possible image pairs. While the speckle pattern is generally better correlated between frames taken close together in time, this is not always the case, especially when comparing frames before and after small telescope nods. Therefore, for each annular section of a science image we want to subtract, we filter reference image sections by their degree of correlation to remove those below a certain, predetermined threshold ( $r_{\text{corr}}$ ).

HR 8799 b is detectable in most individual processed frames (SNR/frame  $\sim 4$ –7), so we measure its position to identify and correct for any astrometric biases caused by a PA “jump” for frames obtained near transit due to imperfect mechanical alignment of the telescope’s  $y$  axis. The position angles of HR 8799 b in frames more than 0.25 hours from transit are consistent, but the PA offset follows a bell-shaped curve with a maximum offset of  $\approx 0.6$  degrees centered on transit. We model and correct for this offset using a fifth-order polynomial. We also reran our pipeline with different rotation axis offsets due to image registration errors, setting an upper limit to this of 0.5 pixels in each coordinate.

Furthermore, unlike the original LOCI algorithm, we set the azimuthal length of the subtraction zone to be smaller (not identical) to the azimuthal length for the optimization zone, equal to  $dr$  (the length along the radial direction). We then center the optimization zone on the subtraction zone. Finally, we iteratively determine the algorithm parameters –  $\delta$ ,  $N_A$ ,  $g$ ,  $dr$  (Lafrenière et al. 2007), and  $r_{\text{corr}}$  – that maximize the signal-to-noise of point sources and applied these settings to extract our

final image<sup>6</sup>.

Figure 1 (right panel) shows our final image displaying higher signal-to-noise detections of HR 8799 b (SNR  $\sim 38$ ) and c (SNR  $\sim 18$ ) and new detection of d (SNR  $\sim 5$ ), using algorithm parameters of  $\delta \geq 0.74$ ,  $N_A = 245$ ,  $g = 0.95$ ,  $dr = 6$ , and  $r_{\text{corr}} \geq 0.315$ , though similar settings yield nearly identical results (i.e.  $\delta \geq 0.73$ –0.8,  $r_{\text{corr}} \geq 0.31$ –0.36). We achieve contrast gains of up to  $\sim 80\%$  (for HR 8799 d) over our best LOCI reduction.

For flux calibration, we perform aperture photometry on HR 8799 bcd and on the nearby star GJ 616.2 observed just prior to HR 8799. We use fake point sources to further correct for LOCI-based photometric biases (i.e. Lafrenière et al. 2007; Currie et al. 2011a,b) and find  $m(H) = 18.05 \pm 0.09$  mag for HR 8799 b,  $m(H) = 17.06 \pm 0.13$  for HR 8799 c, and  $m(H) = 16.71 \pm 0.24$  for HR 8799 d. The magnitude differences between HR 8799 c and d appear slightly discrepant compared to better calibrated NIRC2 measurements from Marois et al. (2008), although the individual measurements are consistent to within  $\sim 1\sigma$ . Photometry derived for HR 8799 bc using classical PSF subtraction agrees with that derived from our A-LOCI based reduction within errors. Bright residual speckles at  $r = 0''.3$ – $0''.4$  prevent detecting HR 8799 e.

## 2.2. October 2010 Data

To supplement the 2005 HR 8799 astrometry, we downloaded and reduced October 2010  $L'$ -band NIRC2 data from the Keck archive (P.I. B. Macintosh). These data are the latest reported by Marois et al. (2010a) who focus on HR 8799 e astrometry: we use these data instead to extract astrometry for HR 8799 bcd. Individual exposures consist of 50s frames totaling  $\approx 80$  minutes taken through transit without a coronagraph with periodic telescope nods for sky subtraction. Observing conditions appeared variable at a level comparable to the July 2005 data and worse than other recent Keck data (i.e. Currie et al. 2012; Rodigas et al. 2012), but we detect all four planets (SNR  $\sim 6$ –20) with our pipeline.

## 3. ASTROMETRIC ANALYSIS AND ORBIT FITTING

### 3.1. Method

We use our detections to better constrain the orbits of HR 8799 bcd, first by fitting the orbits of the planets separately, then identifying the subset of orbits consistent with systematically more stable mean motion resonance configuration. We calibrate our astrometry by assessing and correcting for biases introduced by LOCI-based processing in the same manner as our photometric calibration, using fake point sources. Using different telescopes and slightly different image processing techniques lead to systematic biases in planet astrometry. To minimize these biases, we restrict ourselves to astrometry from HST/1998 (Soummer et al. 2011), Subaru/2002 and 2009 (Fukagawa et al. 2009; Currie et al. 2011a), Keck/2004, 2005, 2007–2009 (Marois et al.

<sup>6</sup> We also considered a “reference PSF library” derived from other 2004–2005 NIRC2 data obtained with the same setup (coronagraph size, filter, etc.) to further attenuate speckles. However, this library degrades the SNR of HR 8799 b and c by  $\approx 30$ –60% and renders HR 8799 d undetectable, because HR 8799’s speckle patterns are poorly correlated with library’s.

2008; Metchev et al. 2009; Galicher et al. 2011, this work), VLT/2009 (Currie et al. 2011a), and LBT/Pisces (Esposito et al. 2012). For the Pisces data, we include the substantial north position angle uncertainty. We furthermore modify the Keck/NIRC2 astrometry reported in Marois et al. (2008) and Metchev et al. (2009) to reflect the updated NIRC2 astrometric calibration (Yelda et al. 2010) accuracy, rescaling the position by a factor of 9.952/9.963, and putting in a  $PA_{\text{north,new}} - PA_{\text{north,old}} = 0.13^\circ$  clockwise rotation.

To separately determine the range of allowable HR 8799 bcd orbits, we follow our previously-adopted Monte Carlo-based approach (Thalmann et al. 2009; Currie et al. 2011b), comparing the HR 8799 planet astrometry to predictions from randomly-selected orbits. In a first set of “conservative” simulations, we consider the orbits separately. Dynamical stability analysis suggests that HR 8799 bcd are likely in resonance (Fabrycky and Murray-Clay 2010); the 4:2:1 resonance is particularly adept at stabilizing the system. To focus on dynamically stable orbits we then select the subset of best-fitting orbits that preclude the planets from crossing orbits and are consistent with a 4:2:1 resonance. Here we define “resonance” broadly, including orbits with ratios of periods between 1.9 and 2.1 for consecutive pairs of planets since, at least in some circumstances, *exact* period ratios may be rare (e.g. Fabrycky et al. 2012)<sup>7</sup>.

For all our simulations, the minimum  $\chi^2$  for the b, c, and d planets are 20.8, 13.8, and 14.8, for reduced  $\chi^2_{\nu}$  values of 1.04, 0.86, and 1.24. Following Currie et al. (2011b), we choose a cutoff of  $\chi^2 \leq \chi^2_{\text{min}} + 1$  to represent the family of best-fitting orbits. Formally, this cutoff admits only an average additional deviation per each x or y measurement of  $\approx 1/2N_{\text{obs}}$  (i.e.  $\approx 1/20$  for HR 8799 b;  $\approx 1/14$  for HR 8799 d) beyond the best-fit models which themselves imply typical deviations of  $\approx 1-\sigma$  per each x or y measurement (since the minimum reduced  $\chi^2_{\nu}$  values are  $\approx 1$ ). However, we obtain nearly identical results for more relaxed cutoffs (see below). From the set of models passing our  $\chi^2$  cutoff, including the subset in resonance, we determine the weighted median value and the weighted 68% confidence interval about the median for each model parameter from amongst the set of best-fitting orbits.

Furthermore, we report a “*most likely orbit*” (MLO) simply defined as follows. First, over the best-fitting family of orbits, we calculate histograms for the following parameters: logarithm of the semi-major axis ( $h_{\log a}$ ), eccentricity ( $h_e$ ), inclination ( $h_i$ ), longitude of ascending node ( $h_{\Omega}$ ), and argument of periastron ( $h_{\omega}$ ). For each orbit  $n$  in the best-fitting ensemble, we then define the measure of likelihood  $\mathcal{L}(n)$  as

$$\mathcal{L}(n) = h_{\log a}(\log a_n) \cdot h_e(e_n) \cdot h_i(i_n) \cdot h_{\Omega}(\Omega_n) \cdot h_{\omega}(\omega_n) \cdot W, \quad (1)$$

i.e., the product of all histograms values in the bins in which the orbit  $n$  lies, representing the individual likelihood of each measured orbital parameter, as well as the statistical weight,  $W$ , representing the likelihood of

<sup>7</sup> Dynamical simulations identify stable solutions for at least *some* planet masses where only HR 8799 c and d are in resonance, so our conclusions from this set of astrometric analyses may be less applicable for HR 8799 b.

the observed planet position within the orbit (i.e., the anomaly)<sup>8</sup>. The most likely orbit is then the one orbit that maximizes the measure of likelihood,  $\mathcal{L}(n_{\text{MLO}}) = \max_n \mathcal{L}(n)$ . Because of the highly skewed distribution of some parameters from the best-fit orbits, in particular  $\log a$ , the MLO parameters can differ significantly from the weighted median parameters.

### 3.2. Results

Table 1 summarizes our results, and Figure 2 displays the orbits in  $a/i/e$  space (left), the histogram distribution of  $i$  (middle), and the histogram distribution of the longitude of the ascending node,  $\Omega$  (right). The top panels display properties for HR 8799 b, the middle for HR 8799 c, and the bottom for HR 8799 d. Assuming a  $\chi^2$  cutoff of  $\chi^2_{\text{min}} + 1$ , the observations well constrain the HR 8799 d orbit –  $a \sim 24\text{--}32$  AU,  $i \sim 32\text{--}42^\circ$ ,  $e \sim 0.03\text{--}0.23$ , and  $\Omega \sim 43\text{--}63^\circ$ . They limit the HR 8799 c’s most plausible orbital parameters to  $a \sim 36\text{--}42$  AU,  $i \sim 13\text{--}26^\circ$ , and  $e \sim 0.03\text{--}0.13$ . As expected, the parameters for HR 8799 b are the most poorly constrained, showing the widest dispersion and the largest differences between the median parameter value and that from the MLO.

Our analysis clearly disfavors face-on orbits for all three planets, especially for HR 8799 c and d. Additionally, the inclination distributions for HR 8799 bc appear systematically skewed towards values lower than those for d. Formally, though, the set of acceptably-fitting orbits HR 8799 bcd include some that make the planets coplanar.

Assuming a 4:2:1 mean-motion resonance configuration, we place far stronger limits on nearly all of the HR 8799 bcd orbital properties (Figure 3). This assumption explicitly rules out  $e > 0.18$  for HR 8799 bc and  $e > 0.3$  for HR 8799 d. Likewise, we identify a very narrow range of planet semimajor axes:  $a = 67.5\text{--}70.8$  AU,  $42.1\text{--}44.4$  AU, and  $26.4\text{--}28.1$  AU for HR 8799 b, c, and d. The 68% confidence interval in  $\Omega$  for HR 8799 d further narrows to  $46^\circ\text{--}62^\circ$ .

For this configuration, HR 8799 d (c) must be in an orbit viewed more than  $25^\circ$  ( $15^\circ$ ) from face-on while HR 8799 b is likely inclined by at least  $5^\circ$ . Furthermore, the inclination distributions between HR 8799 d and HR 8799 bc are even more dissimilar, implying that HR 8799 d is most likely inclined relative to c by at least  $\approx 7^\circ$  and b by more than  $\approx 21^\circ$ . While our analyses cannot conclusively rule out coplanar orbits in a 4:2:1 mean-motion resonance, they suggest that few such orbits are compatible with 12 years of HR 8799 planet astrometry.

To confirm that we are fully sampling the subset of orbital parameters covering the  $\chi^2$  minima, we run our simulations with a more relaxed  $\chi^2$  cutoff of  $\chi^2 \leq \chi^2_{\text{min}} + [5, 5, 3.5]$  for HR 8799 b, c, and d, which formally admit an additional average deviation from the data of  $\approx 0.3\text{--}\sigma$  for each measurement. With this cutoff, we obtain nearly identical results (second set of rows in Table 1). Considering the planets’ orbits separately, we find  $a \sim 23\text{--}31$  AU,  $i \sim 27\text{--}41^\circ$ ,  $e \sim 0.01\text{--}0.31$ , and  $\Omega \sim 41\text{--}53^\circ$  for HR 8799d. We find similar ranges in orbital parameters for HR 8799 c and (for the resonance case) HR 8799

<sup>8</sup> Here, the statistical weight  $W$  is defined as the mean orbital velocity for the corresponding orbit divided by the orbital velocity at the observed epoch,  $W := \langle v \rangle_{\text{orbit}} / v(t_{\text{obs}})$ .

b. Likewise, the planets’ range of inclinations exclude face-on orbits. HR 8799 d’s inclination distribution is skewed to systematically higher values, expected if it is non-coplanar with b and c, although here there are more orbit combinations that could make the planets coplanar.

#### 4. DISCUSSION

From analyzing HR 8799 bcd astrometry from our new “pre-discovery” image and other data, we provide new constraints on the planets’ orbital properties. Treating the three planets separately, we narrowly constrain three major orbital parameters ( $a/i/e$ ) for HR 8799 c and d. None of the planets are likely to be orbiting face-on and the inclinations for acceptably-fitting orbits are systematically higher for HR 8799 d than for HR 8799 b and c.

If HR 8799 bcd have semimajor axes consistent with a 4:2:1 resonance, our analysis strongly constrains the major orbital properties for all three planets. The three planets (especially c and d) then even more obviously have inclined orbits. Most acceptable solutions for HR 8799 d place the planet on an orbit inclined by more than  $7^\circ$  ( $21^\circ$ ) relative to HR 8799 b(c)’s orbit: few orbital solutions consistent with the astrometry also place them on coplanar orbits. Adopting a less restrictive definition for “acceptably-fitting” orbits does not undo any of these trends, although there are more orbit combinations making the planets coplanar. Adopting the median parameter value or MLO instead of the more conservative 68% confidence interval likewise does not change these results.

These results provide valuable input for constraining the mass of the HR 8799 planetary system. Longer-term

astrometric monitoring of HR 8799 (i.e. Konopacky et al. 2011) will better clarify the planets’ orbital properties. Limits on the planets’ dynamical masses will provide crucial input for planet cooling models and even more firmly establish HR 8799 as a benchmark system to understand the properties of young, self-luminous planets.

Finally, this work and other recent studies of HR 8799 (Soummer et al. 2011; Lafrenière et al. 2009; Fukagawa et al. 2009) clearly demonstrate the value of publicly archiving data on advanced telescopes. In our case, detecting at least two HR 8799 planets (HR 8799 bc) was rather straightforward and did not require advanced image processing techniques developed well after the data were taken. As data for Keck and many other 8–10 m class telescopes are now archived, they provide an indispensable resource with which to confirm and characterize directly imaged planets like HR 8799’s and other substellar companions.

We thank Christian Marois, Scott Kenyon, and the anonymous referee for helpful comments. This research has made use of the Keck Observatory Archive (KOA), which is operated by the W. M. Keck Observatory and the NASA Exoplanet Science Institute (NExSci), under contract with the National Aeronautics and Space Administration. We are extremely grateful to the NExSci/KOA staff for developing and maintaining the NIRC2 archive. TC is supported by a NASA Postdoctoral Fellowship; SM is supported by an Astronomy Center for Theory and Computation Prize Fellowship at the University of Maryland.

#### REFERENCES

- Currie, T., Bailey, V., et al., 2010, *ApJ*, 721, 177L  
 Currie, T., Burrows, A., et al., 2011, *ApJ*, 729, 128  
 Currie, T., Thalmann, C., et al., 2011, *ApJ*, 736, 33L  
 Currie, T., Rodigas, T., et al., 2012, *ApJ* submitted, arXiv:1206.4688  
 Esposito, S., et al., 2012, *A&A* submitted, arXiv:1203.2735  
 Fabrycky, D., Murray-Clay, R., 2010, *ApJ*, 710, 1408  
 Fabrycky, D., et al., 2012, *ApJ* submitted, arXiv:1202.6328  
 Fukagawa, M., et al., 2009, *ApJ*, 696, 1L  
 Galicher, R., et al., 2011, *ApJ*, 739, 41L  
 Konopacky, Q., et al., 2011, *BAAS*  
 Lafrenière, D., et al., 2007, *ApJ*, 660, 770  
 Lafrenière, D., et al., 2009, *ApJ*, 694, 148L  
 Madhusudhan, N., Burrows, A., Currie, T., 2011, *ApJ*, 737, 34  
 Marois, C., et al., 2006, *ApJ*, 641, 556  
 Marois, C., et al., 2008, *Science*, 322, 1348  
 Marois, C., et al., 2010a, *Nature*, 468, 1080  
 Marois, C., et al., 2010b, *SPIE*, 7736, 52  
 Metchev, S., Marois, C., Zuckerman, B., 2009, *ApJ*, 705, 204L  
 Rodigas, T. J., et al., 2012, *ApJ*, 752, 57  
 Soummer, R., et al., 2011, *ApJ*, 741, 55  
 Spiegel, D., Burrows, A., 2012, *ApJ*, 745, 174  
 Sudol, J., Haghighpour, N., 2012, *ApJ* in press, arXiv:1201.0561  
 Thalmann, C., et al., 2009, *ApJ*, 707, 123L  
 Yelda, S., et al., 2010, *ApJ*, 725, 331  
 Zuckerman, B., et al., 2011, *ApJ*, 732, 61

TABLE 1  
HR 8799 PLANET PHOTOMETRIC/ASTROMETRIC PROPERTIES

Parameter	HR 8799 b	HR 8799 c	HR 8799 d
<b>Measured</b>			
<i>Photometry</i>			
$m(H)$ on 2005-07-15	18.05 ± 0.09	17.06 ± 0.13	16.71 ± 0.24
<i>Astrometry</i>			
2005-07-15 ([E,N])''	1.496, 0.856 (± 0.005)	-0.713, 0.630 (± 0.005)	-0.087, -0.578 (± 0.010)
2010-10-30 ([E,N])''	1.546, 0.748 (± 0.005)	-0.598, 0.737 (± 0.005)	-0.283, -0.567 (± 0.005)
<b>Derived</b>			
<i>MLO, med., [68% C.I.]</i>			
$(\chi_{\text{lim}}^2 \leq \chi_{\text{min}}^2 + 1)$			
$a$ (AU), full	71.0, 109.9 [69.7,164.9]	37.2, 38.0 [35.5,42.0]	26.2, 27.3 [24.4,31.5]
// 4:2:1 resonance	68.1, 68.8 [67.5,70.8]	42.5, 43.2 [42.1,44.4]	27.3, 27.3 [26.4,28.1]
$i$ (°), full	14.1, 34.9 [12.3,43.0]	21.7, 19.9 [12.5,25.8]	37.1, 37.9 [31.6,41.6]
// 4:2:1 resonance	8.5, 9.5 [4.9,14.8]	25.8, 27.6 [25.2,28.8]	38.1, 37.9 [36.0,39.1]
$e$ , full	0.02, 0.27 [0.02,0.49]	0.01, 0.08 [0.03,0.13]	0.04, 0.09 [0.03,0.23]
// 4:2:1 resonance	0.01, 0.02 [0.0,0.03]	0.12, 0.14 [0.11,0.17]	0.03, 0.04 [0.01,0.08]
$\Omega$ (°), full	149.7, 141.0 [40.9,161.4]	128.8, 122.2 [62.0,152.4]	56.8, 53.5 [43.3,63.0]
// 4:2:1 resonance	163.2, 87.1 [22.9,158.9]	147.4, 131.9, [104.8,158.5]	56.9, 54.3 [46.0,60.2]
$(\chi_{\text{lim}}^2 \leq \chi_{\text{min}}^2 + [5,5,3.5])$			
$a$ (AU), full	70.7, 80.8 [68.2,117.2]	38.2, 39.8 [36.6,46.2]	26.2, 27.0 [23.0,31.0]
// 4:2:1 resonance	68.0, 68.5 [66.4,71.0]	42.7, 42.9 [41.3,44.6]	27.3, 27.1 [26.0,28.2]
$i$ (°), full	15.2, 24.5 [10.4,36.6]	19.7, 23.2 [14.0,31.3]	38.1, 36.9 [27.1,41.2]
// 4:2:1 resonance	10.8, 11.5 [6.1,17.1]	28.8, 27.4 [24.6,30.2]	37.1, 37.7 [34.6,39.9]
$e$ , full	0.01, 0.13 [0.02,0.34]	0.01, 0.07 [0.02,0.15]	0.01, 0.15 [0.04,0.32]
// 4:2:1 resonance	0.01, 0.03 [0.01,0.06]	0.02, 0.09 [0.02,0.14]	0.0, 0.05 [0.01,0.11]
$\Omega$ (°), full	142.7, 119.5 [32.4,160.5]	124.7, 86.8 [37.1,142.5]	52.5, 58.4 [41.0,98.5]
// 4:2:1 resonance	142.1, 78.2 [21.9,154.3]	61.1, 70.5 [42.2,140.5]	60.9, 55.7 [44.1,67.2]

NOTE. — *Measured parameters* – Our photometric uncertainties consider both the signal-to-noise of our detections and the absolute flux calibration uncertainties; astrometric uncertainties consider the SNR, astrometric calibration uncertainty (e.g. 0.5 pixels in  $x$  and  $y$ , see Sect. 2), etc. *Derived parameters* – The three column entries are *MLO* (the “most likely orbit” (see §3)), *med.* (the median parameter value), and *[68% C.I.]* (the 68% confidence interval).

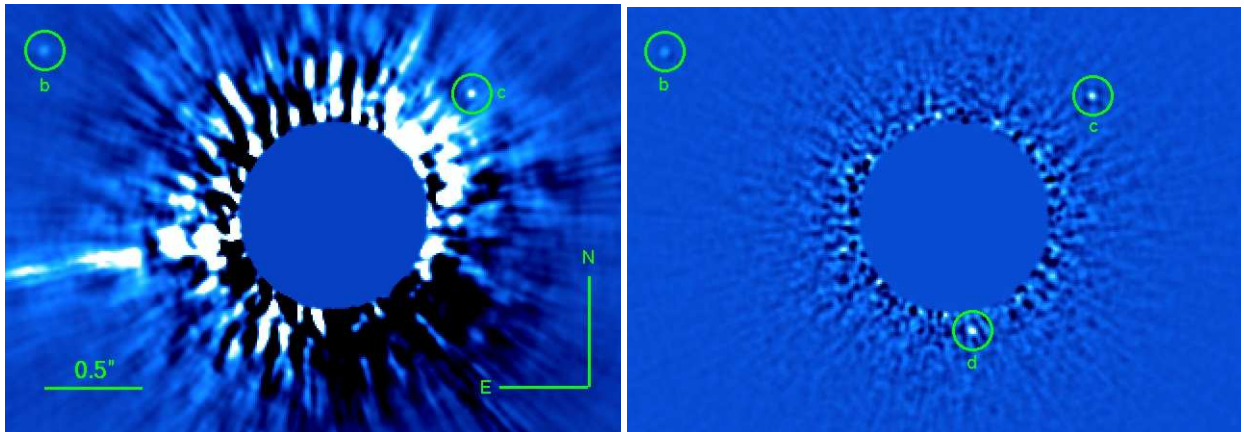


FIG. 1.— HR 8799 images processed with “classical” PSF subtraction (left) and A-LOCI (right) showing the detections of HR 8799  $b$ ,  $c$ , and  $d$  (circled).

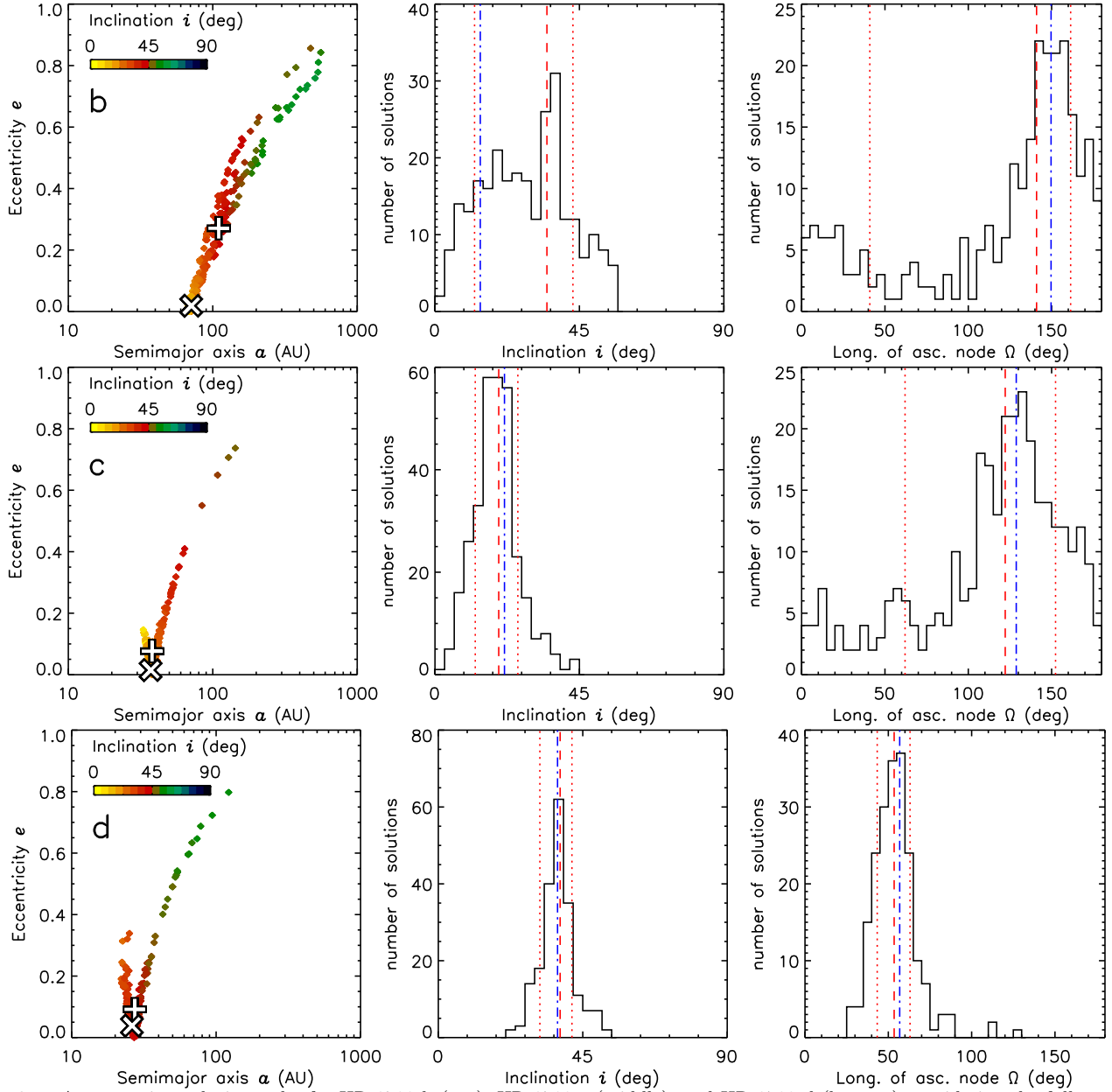


FIG. 2.— Astrometric analysis results for HR 8799 b (top), HR 8799 c (middle), and HR 8799 d (bottom) considering the full range of orbits satisfying the criterion  $\chi^2_\nu < \chi^2_{\nu, \min} + 1$ . The panels show the orbits in  $a/e/i$  space (left) and histogram distributions of the orbital inclination  $i$  (middle panels) and longitude of ascending node (right panels). In the left panels, the ‘x’ identifies parameters  $e$  and  $a_p$  from the best-fit orbital solution; the ‘plus’ sign denotes the weighted median value for the same parameters. For the middle and right panels, the vertical blue dashed line identifies the MLO, the vertical red dashed line identifies the median parameter value, and the vertical red dotted lines bracket the 68% confidence interval.

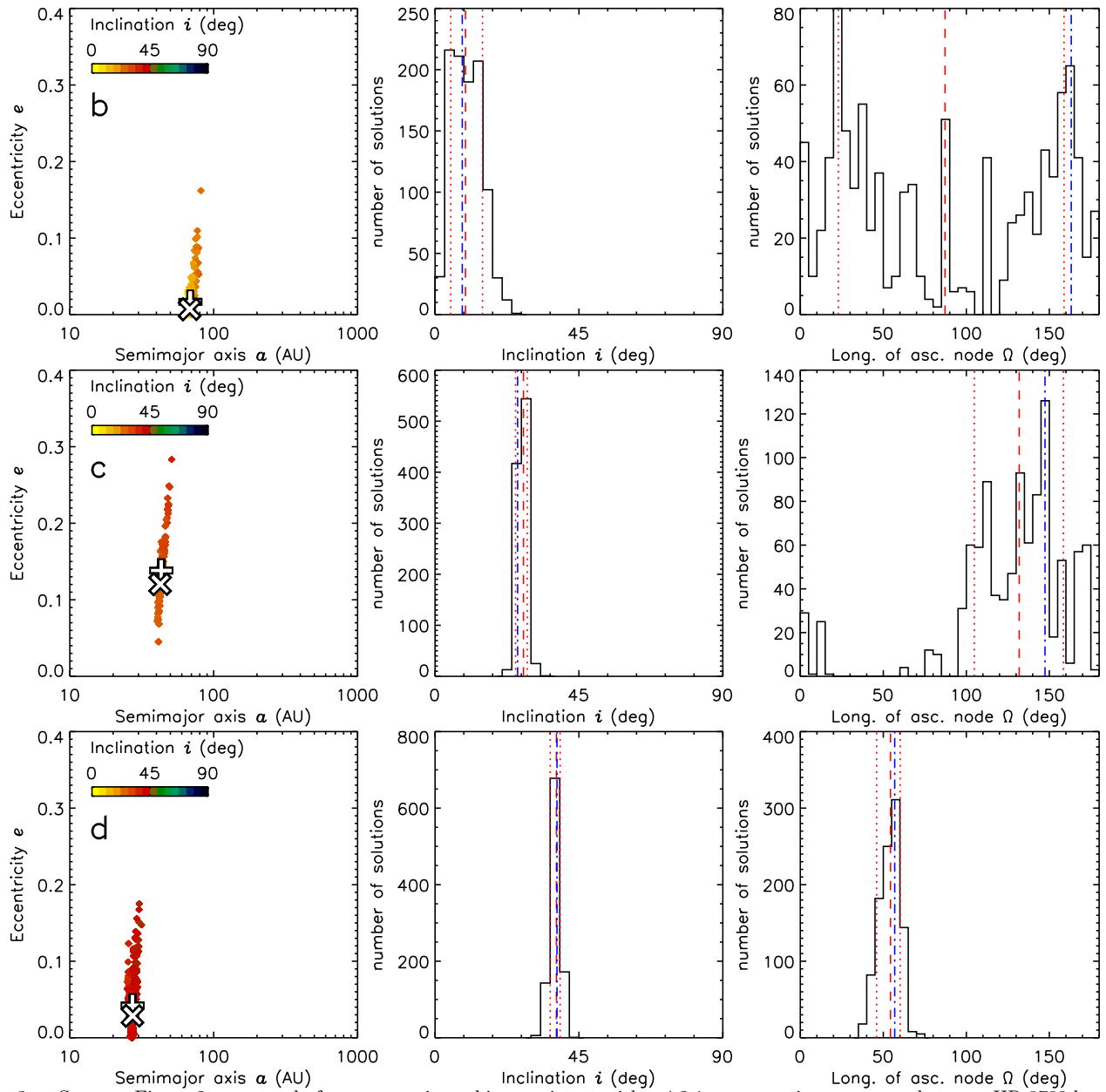


FIG. 3.— Same as Figure 2 except only for non-crossing orbits consistent with a 4:2:1 mean-motion resonance between HR 8799 b, c, and d, a configuration which promotes orbital stability (e.g. Fabrycky and Murray-Clay 2010). Note the lack of high-eccentricity orbits and the narrower range in acceptable orbital parameters, especially for HR 8799 c and d.